RESEARCH PAPER

PCCP
www.rsc.org/pccp

Ab initio study of the fluoride–ammonia clusters: F^-–$(NH_3)_n$, $n = 1$–3†

D. A. Wild* and T. Lenzer

MPI für biophysikalische Chemie, Abteilung 010, Am Faßberg 11, D-37077 Göttingen, Germany. E-mail: dwild@gwdg.de, tlenzer@gwdg.de; Fax: +49 551 201 1501; Tel: +49 551 201 2004

Received 11th August 2004, Accepted 15th September 2004
First published as an Advance Article on the web 8th October 2004

Fluoride–ammonia clusters have been investigated *via ab initio* calculations at the MP2 level of theory, using Dunning's augmented correlation consistent basis sets. Optimised geometries, vibrational frequencies, and enthalpy changes for the ligand association reactions are presented for clusters with one, two, and three ammonias bound to a fluoride anion. The minimum energy structure for the F^-–NH_3 complex, with C_s symmetry, displays a single hydrogen bond between the ammonia and fluoride anion. For the F^-–$(NH_3)_2$ cluster, two closely lying minima with C_2 and C_1 symmetry were predicted. For F^-–$(NH_3)_3$, four minima were located, with the minimum energy structure having C_{3h} symmetry. Calculated infrared spectra for the minima are presented to aid in assigning spectra from future experimental studies.

1. Introduction

Much progress has been made in recent years towards understanding the interactions between ions and solvent molecules. Such endeavours have obvious importance for more detailed descriptions of molecular interactions, and for describing ion solvation in bulk contexts.[1] Advances have been made in both experimental and theoretical methodologies. On the experimental front, photoelectron, infrared, and microwave spectroscopy of gas phase ion complexes and clusters have furnished qualitative, or in some cases quantitative, structural information.[2–23] *Ab initio* calculations of ion–solvent complexes have proved useful in rationalising experimental observations, and in guiding future experiments.[24–27]

Due to its obvious importance, the solvation of ions (particularly halide anions) by water has received much attention. Both experiment[15,16,28–30] and theory[28,31–35] concur that the structures adopted by halide–water clusters depend on the balance of ion–solvent and solvent–solvent interactions. For example, in the fluoride–water clusters the anion–solvent binding forces dominate, resulting in the anion being situated in the interior of the structure.[28] For clusters involving the larger halides, the solvent–solvent attractive interactions play a more significant role in determining the cluster structure, the result being solvent–solvent bonds and asymmetric structures where the anion binds to the surface of the solvent network. Experimental evidence, provided by IR spectra of Johnson and co-workers, was the absence of bands in the spectra due to free or non-bonded O–H oscillators,[29] and the introduction of ring modes similar to those seen for the neutral water trimer.[36,37] For a recent review on investigations of halide ion hydration, see ref. 38.

The halide–ammonia clusters have received relatively little attention compared to the analogous halide–water species. Selected complexes have been probed *via* high pressure mass spectrometry,[39] photoelectron spectroscopy,[40,41] vibrational predissociation spectroscopy,[42] and time resolved photoelectron spectroscopy.[43] Castleman and co-workers performed high pressure mass spectrometry experiments on the chloride, bromide, and iodide–ammonia complexes and reported enthalpy changes for the association reactions of −8.2, −7.7, and −7.4 kcal mol^{-1}, respectively. The association reaction enthalpy change for the F^-–NH_3 complex was estimated to be −11 kcal mol^{-1} from comparison of extrapolated and calculated values.[39]

Kaldor and co-workers applied photoelectron spectroscopy to the chloride–ammonia complex,[41] and complemented this work with *ab initio* calculations at the CCSD level with a truncated ANO basis set for chloride and fluoride–ammonia.[40] A binding energy of 0.36 eV (8.3 kcal mol^{-1}) was reported for the chloride–ammonia complex in very good agreement with the work of Castleman and co-workers. The complexes were predicted to have a C_s structure featuring a single hydrogen bond between the anion and ammonia.

Bieske and co-workers investigated the chloride–ammonia complex *via* vibrational predissociation spectroscopy.[42] The infrared spectrum and supporting *ab initio* calculations at the MP2/aug-cc-pVTZ level of theory were consistent with the structure predicted by Kaldor.[40] Three other stationary points were predicted; the C_s and C_{2v} transition states, and the C_{3v} second order stationary point. The transition states correspond to tunnelling motion of the ammonia molecule between equivalent C_s minima. The barrier to 'turnstile' tunnelling of the ammonia (*via* the C_s bifurcated transition state) was predicted to be 1.72 kcal mol^{-1}, while the barrier to umbrella inversion of the ammonia molecule (*via* the planar C_{2v} transition state) was estimated as 5.23 kcal mol^{-1}.

Neumark and co-workers applied time resolved photoelectron spectroscopy to I^-–$(NH_3)_n$ clusters ($n = 4$–15).[43] They investigated the dynamics associated with the excitation of the charge-transfer-to-solvent (CTTS) precursor states. The spectra implied that electron solvation, *via* solvent rearrangement, occurs on a timescale of 0.5–2 ps following photoexcitation.

To date, there have been no reported electronic structure calculations or infrared spectra of the larger halide–ammonia clusters which are essential for defining cluster structures. The current work constitutes an investigation of smaller

† Electronic supplementary information (ESI) available: Scan data along the association coordinate of the C_s minimum. Scan data for higher order stationary points. (Tables S1 and S2). See http://www.rsc.org/suppdata/cp/b4/b412414f/

DOI: 10.1039/b412414f

fluoride–ammonia clusters, with up to three ammonias bound to a fluoride anion. We wish to determine whether symmetric or asymmetric solvation structures are preferred. Furthermore, we aim to provide vibrational frequencies that might prove helpful for future experimental studies. Our choice of computational methodology is guided by previous studies of the water–halide clusters. It has been shown that the MP2/aug-cc-pVxZ (x = D, T) calculations are good choices for describing the halide–water systems.[28,31,34,35,44–46] Furthermore, the same methodology has been used for the ammonia dimer, adequately describing the ammonia–ammonia hydrogen bond.[47]

2. Methodology

The fluoride–ammonia clusters were investigated at the MP2 level of theory using Dunning's augmented correlation consistent polarized valence sets.[48–50] For the F^-–NH_3 complex, calculations were performed with basis sets of double, triple, and quadruple-ζ quality (aug-cc-pVxZ where x = D, T, Q). HF and MP4(SDQ) geometry optimisations were performed to consider the effect of electron correlation. Only the valence electrons were correlated in the MP2 and MP4 calculations. MP2/aug-cc-pVDZ and MP2/aug-cc-pVTZ calculations were undertaken for F^-–$(NH_3)_2$, while MP2/aug-cc-pVDZ calculations were performed for F^-–$(NH_3)_3$ clusters. All optimisations were performed using 'Very Tight' convergence criteria, as it is expected that the potential energy surfaces will be quite flat especially for the n = 2 and 3 clusters. Corrections to the intermolecular interaction energy arising from basis set superposition error (BSSE) were estimated using the method of Boys and Bernardi.[51] Harmonic vibrational frequencies were computed analytically at the same level of theory used for the geometry optimisations. It should be remembered that the calculated vibrational frequencies overestimate the actual frequencies, due to not taking anharmonicity into account. NBO analyses were performed on the clusters to determine the extent of H-bonding.[52] Enthalpy changes for the ligand association reactions at 298 K were estimated using the method described in ref. 53. The geometry optimisations, energy and vibrational frequency calculations, and NBO analyses were performed with the GAUSSIAN-03 program suite.[54] Diagrams of the cluster structures were produced using gOpenMol.[55,56]

3. Results/discussion

A. F^-–NH_3

Four stationary points were located for the fluoride–ammonia complex. The points, shown in Fig. 1, correspond to the C_s minimum energy structure, C_s and C_{2v} first order transition states, and the C_{3v} second order stationary point. Calculated

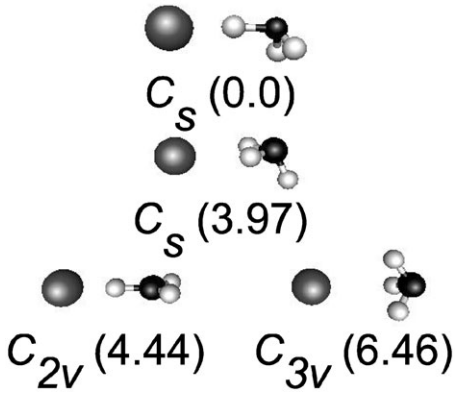

Fig. 1 Four stationary points calculated for the F^-–NH_3 complex. Also provided are the energy differences between the stationary points, with zero point energies difference corrections (in kcal mol^{-1}). Optimal internal coordinates appear in Table 2.

Table 1 Calculated internal coordinates and energies of the F^-–NH_3 complex at the HF, MP2 and MP4(SDQ) levels of theory with aug-cc-pVxZ basis sets (x = D, T, Q). Bond lengths are in Å, angles in degrees, and energies in atomic units. H_b refers to the H-bonded hydrogen, H_t are the terminal hydrogens

	aug-cc-pVDZ	aug-cc-pVTZ	aug-cc-pVQZ
HF			
$r(F^-–H_b)$	1.719	1.718	1.720
$r(N–H_b)$	1.035	1.030	1.030
$r(N–H_t)$	1.006	1.001	1.001
$\theta(F^-–H_b–N)$	173.5	173.6	173.6
$\theta(H_b–N–H_t)$	105.6	106.2	106.2
$\theta(H_t–N–H_t)$	105.4	105.9	106.0
E_e	−155.655166	−155.692319	−155.702681
MP2			
$r(F^-–H_b)$	1.604	1.586	1.585
$r(N–H_b)$	1.072	1.067	1.065
$r(N–H_t)$	1.023	1.015	1.013
$\theta(F^-–H_b–N)$	176.4	176.3	176.1
$\theta(H_b–N–H_t)$	104.8	105.1	105.2
$\theta(H_t–N–H_t)$	104.2	104.5	104.6
E_e	−156.096557	−156.232521	−156.278241
MP4(SDQ)			
$r(F^-–H_b)$	1.635	1.621	
$r(N–H_b)$	1.064	1.058	
$r(N–H_t)$	1.025	1.016	
$\theta(F^-–H_b–N)$	175.6	175.4	
$\theta(H_b–N–H_t)$	104.7	105.0	
$\theta(H_t–N–H_t)$	104.1	104.5	
E_e	−156.110769	−156.240251	
CCSD[a]	ANO		
$r(F^-–H_b)$	1.626		
$r(N–H_b)$	1.056		
$r(N–H_t)$	1.018		
$\theta(F^-–H_b–N)$	175.6		
$\theta(H_b–N–H_t)$	105.0		
$\theta(H_t–N–H_t)$	104.5		

[a] Results of CCSD calculations taken from ref. 40.

data are provided in Tables 1 and 2, including internal coordinates, vibrational frequencies, energies, and for the C_s minimum the enthalpy change for the ligand association reaction at 298 K.

I. C_s minimum. The C_s minimum energy complex was investigated by HF and MP2 methods with basis sets of double, triple, and quadruple-ζ quality, and by the MP4(SDQ) method using basis sets of double and triple-ζ quality. The results of these calculations are given in Table 1. One can see that increasing the level of electron correlation from HF to MP2 to MP4 affects the predicted structure. Using calculations with the aug-cc-pVTZ basis set as an example, the intermolecular bond length shortens on going from HF to MP2 theory (Δr = −0.132 Å), and increases slightly on going from MP2 to MP4 (Δr = +0.035 Å). The F^-–H_b–N angle increases from HF to MP2 ($\Delta\theta(F^-–H_b–N)$ = +2.7°), and then decreases on going from MP2 to MP4 ($\Delta\theta(F^-–H_b–N)$ = −0.9°). The differences between the MP2 and MP4 calculations are not so large, leading us to believe that MP2 method is adequate in describing the systems, and has the advantage of reduced computation times. From the MP2 calculations it can be seen that increasing the basis set size above triple-ζ quality results in only slight changes to the structure (Δr = 0.002 Å and $\Delta\theta$ = 0.2°), therefore this basis set is considered to be a good choice to describe the system. The following discussion of the 1 : 1 complex will concentrate on the MP2/aug-cc-pVTZ results.

In agreement with the previous theoretical study of Kaldor,[40] the minimum energy structure for the fluoride–ammonia

Table 2 Calculated data for the minimum energy structure and transition states of F^-–NH_3 at MP2/aug-cc-pVTZ. Provided are internal coordinates (r in Å and θ in degrees), harmonic vibrational frequencies (ω in cm^{-1}, symmetries included, intensities in km mol^{-1} in bold font style), *zpe* (in kcal mol^{-1}), MP2 energies (E_{MP2} in hartrees), BSSE and *zpe* corrected energy differences ($\Delta E_{BSSE/Corr}$ in kcal mol^{-1}), and enthalpy change for the association reaction at 298 K ($\Delta H_{0\rightarrow 1}^{298}$ in kcal mol^{-1}). Also, provided are data for bare NH_3 and F^- from MP2/aug-cc-pVDZ and MP2/aug-cc-pVTZ calculations

	C_s min	C_s	C_{2v}	C_{3v}
$r(F^-–H_b)$	1.586	2.220	1.515	2.530
$r(N–H_b)$	1.067	1.022	1.068	1.019
$r(N–H_t)$	1.015	1.015	1.000	
$\theta(F^-–H_b–N)$	176.3	112.8	180.0	49.9
$\theta(H_b–N–H_t)$	104.5	104.6	122.2	
$\theta(H_t–N–H_t)$	105.1		115.6	
ω_1	3510 a' **17**	3588 a'	3689 a_1	3476 a_1
ω_2	2685 a' **1615**	3445 a'	2556 a_1	1285 a_1
ω_3	1644 a' **6**	1638 a'	1517 a_1	169 a_1
ω_4	1257 a' **74**	1256 a'	299 a_1	3550 e
ω_5	508 a' **55**	316 a'	954 b_1	1680 e
ω_6	283 a' **111**	202 a'	709i b_1	321i e
ω_7	3598 a'' **3**	3491 a''	3806 b_2	
ω_8	1725 a'' **5**	1641 a''	1659 b_2	
ω_9	414 a'' **15**	411i a''	389 b_2	
zpe	22.4	22.3	21.3	22.0
E_{MP2}	−156.232521	−156.223801	−156.223734	−156.220874
$\Delta E_{BSSE/Corr}$	(0.0)	3.97	4.44	6.46
$\Delta H_{0\rightarrow 1}^{298}$	−15.8			
		NH_3		
	aug-cc-pVDZ	aug-cc-pVTZ		
$r(N–H)^a$	1.020(+8)	1.012(0)		
$\theta(H–N–H)^a$	106.3(−4)	106.8(+1)		
ω_1 (a_1)	3480 **5**	3503 **3**		
ω_2 (a_1)	1045 **131**	1037 **139**		
ω_3 **(e)**	3635 **5**	3650 **8**		
ω_4 **(e)**	1649 **13**	1669 **14**		
Zpe	21.6	21.7		
E_{MP2}	−56.404890	−56.460541		
		F^-		
E_{MP2}	−99.665948	−99.745879		

[a] Numbers in parentheses are differences in the last sig. fig. between these calculations and experimental values taken from ref. 57.

complex is one with the ammonia bound to the fluoride anion *via* a single, nearly linear hydrogen bond ($\theta(F^-–H_b–N)$ = 176.3°). Compared to the CCSD calculations,[40] the intermolecular bond length from our MP2/aug-cc-pVTZ calculations is contracted (1.586 *vs.* 1.626 Å), and closer to linearity (176.3 *vs.* 175.6°). The calculated enthalpy change for the ligand association reaction (at 298 K) is −15.8 kcal mol^{-1}. This is somewhat higher than the value estimated by Castleman and co-workers of −11 kcal mol^{-1}.[39]

Complex formation with F^- affects the ammonia in a number of ways, most noticeably by elongation of the H-bonded N–H bond (Δr = +0.055 Å from Table 2), and further distortion of the ammonia molecule from planarity ($\Delta\theta$(H–N–H) = −1.7 and −2.3°). The non-bonded N–H bond lengths are slightly elongated relative to bare ammonia (Δr = +0.003 Å).

II. Other stationary points. We turn our attention now to the three other stationary points of the 1 : 1 complex (Table 2, Fig. 1). Firstly, the C_s structure involves a double hydrogen bond (confirmed by NBO analysis, *vide infra*) between the ammonia and fluoride, and corresponds to the 'turnstile' tunnelling transition state between equivalent singly bound C_s minima. After BSSE and *zpe* corrections are made, the energy difference between this transition state and the C_s minimum, or effectively the barrier to tunnelling along this coordinate, is estimated to be 3.97 kcal mol^{-1} or 1600 cm^{-1}. The fluoride–ammonia complex is more rigid along this coordinate than Cl^-–NH_3 which has a tunnelling barrier of 1.66 kcal mol^{-1}, an effect of the stronger H-bond for the minimum.[42] The planar C_{2v} transition state involves a single H-bond between ammonia and fluoride (see NBO analysis), and corresponds to 'umbrella' inversion of the NH_3 molecule. The calculations predict a smaller barrier of 4.44 kcal mol^{-1} for the fluoride–ammonia complex compared to 5.23 kcal mol^{-1} for Cl^-–NH_3.[42] Finally, the C_{3v} structure is a second order stationary point, with a doubly degenerate imaginary frequency (321i cm^{-1}) corresponding to the rocking motion towards one of the three equivalent hydrogens. This structure lies some 6.46 kcal mol^{-1} to higher energy from the C_s minimum, while for Cl^-–NH_3 the energy difference is only 2.24 kcal mol^{-1}.[42] This difference may arise from the shorter intermolecular distance in the fluoride complex (2.530 *vs.* 3.053 Å),[42] leading to a more repulsive interaction in this configuration compared with the chloride complex.

III. NBO analyses. NBO analyses were performed to assess the nature of the hydrogen bond in the predicted structures. The results of the analysis constitute molecular orbital occupancies (in *me*) and second-order perturbation energies $E^{(2)}$ for electron density donor → acceptor interactions (in kcal mol^{-1}). The signature of H-bonding is electron density transfer from the lone pairs of the H-bond acceptor (F^-), to the anti-bonding orbitals of the H-bond donor (NH_3).

The results of the NBO analysis for the C_s structure reveal significant electron density transfer from the lone pairs of the fluoride anion to anti-bonding orbital associated with the H-bonded N–H group. In total, 52 *me* of electron density is

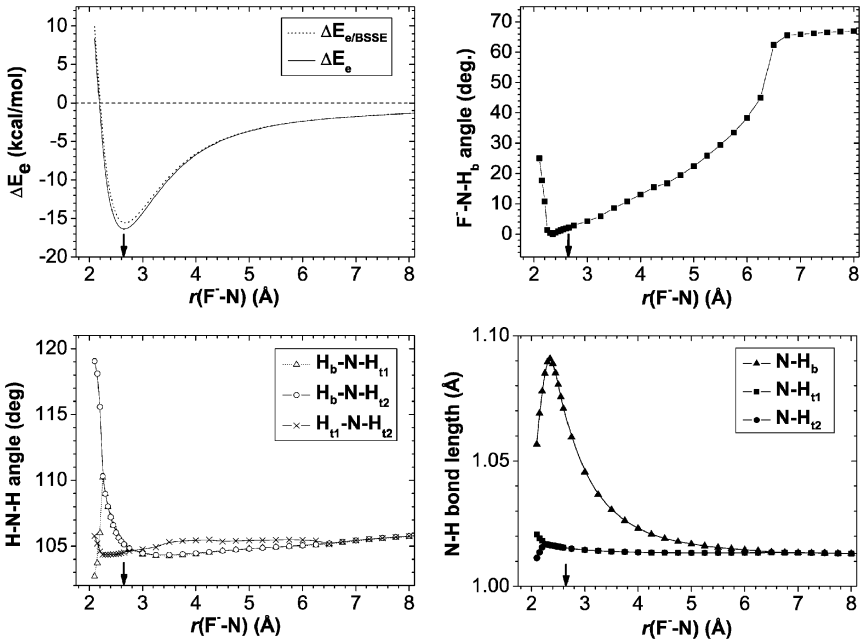

Fig. 2 Changes in the energies and internal coordinates of the F^-–NH_3 complex along the association coordinate $r(F^-–N)$. The position of the minimum is marked on each plot with an arrow. See text for details, and supplementary material† for data.

transferred. An NBO analysis was also performed on the ammonia molecule in the complex geometry with the fluoride anion replaced with a point charge to determine the change in orbital occupancies due to polarisation by the negative charge. This analysis reveals that a very small portion, *ca.* 10 μe, is due to polarisation of the ammonia molecule by the anion. The second-order perturbation energies $E^{(2)}$, or effectively the stabilisation energies resulting from the electron density transfer, reveal that the transfer from the lone pairs of the fluoride anion affords the greatest stabilisation. The total value is 41.7 kcal mol^{-1} for transfer from the fluoride lone pairs to the antibonding orbital.

NBO analyses were also performed for the higher order stationary points shown in Fig. 1. For the double H-bonded C_s structure, the analysis confirmed the double H-bond between anion and ammonia with electron density transfer from lone pairs of the fluoride anion to the two N–H antibonding orbitals. The orbital occupancy and stabilisation energy $E^{(2)}$ (donor → acceptor) is *ca.* 2.5 *me* and 0.83 kcal mol^{-1}, respectively, for each orbital. The C_{3v} structure features a triple H-bond from the anion to the ammonia, although in this instance the bond strengths are much weaker. The orbital occupancy is predicted to be 0.38 *me* per orbital, while the stabilisation energy is 0.07 kcal mol^{-1}. Finally, the C_{2v} planar structure exhibits the strongest H-bond of all the geometries. The N–H antibonding orbital occupancy is predicted to be 66.25 *me*, while the stabilisation energy is 51.88 kcal mol^{-1}. The strength of this H-bond is not surprising if one considers that the F^-–H_b–N intermolecular angle is 180°, and hence the lone pair-antibonding orbital alignment is maximised. The H-bond strength is seen to decrease in the order $C_{2v} > C_s$ min > $C_s > C_{3v}$ in proportion to the intermolecular angle $\theta(F^-–H_b–N)$ = 180, 176.3, 112.8, and 49.9°, respectively (Table 2).

IV. 1-D intermolecular potentials. To further characterise the fluoride–ammonia interaction, a relaxed scan along the association coordinate, $r(F^-–N)$, was undertaken at the MP2/aug-cc-pVTZ level of theory. The results of this scan in terms of internal coordinates and energies are presented in Fig. 2, with the intermolecular bonding angle now defined as $\theta(F^-–N–H_b)$. Data from the scan can be found in the Electronic Supplementary Information.† At large intermolecular separations, the fluoride ammonia interaction is dominated by the electrostatic interaction between the ion and the ammonia dipole moment, leading to an F^-–N–H_b angle of approximately 67°. As the fragments move closer together, the complex adopts a single hydrogen bond, moving towards the C_s minimum energy structure shown in Fig. 1 ($\theta(F^-–N–H_b)$ = 2.2° at $r(F^-–N)$ = 2.651 Å). The change in the bond lengths and angles of the ammonia molecule are shown in Fig. 2. The ammonia bond lengths elongate, while the H–N–H angles decrease. Finally, at very short intermolecular separations, the ammonia twists into a strained geometry where the F^-–N–H angle increases again ($\theta(F^-–N–H)$ = 25° at $r(F^-–N)$ = 2.1 Å) as the H-bonded hydrogen points away from the anion.

One-dimensional potential energy curves describing the interaction between the fluoride and ammonia along the association coordinate $r(F^-–N)$ were also developed for the C_s and C_{3v} stationary points. The purely repulsive interaction where the fluoride approaches the nitrogen of the ammonia, in a C_{3v} symmetry arrangement, was also considered. The curves are provided in Fig. 3, and the data for these scans in terms of energy differences (ΔE_e) and BSSE corrected energy differences ($\Delta E_{e/BSSE}$) are given in the Electronic Supplementary Information.† These 1-D intermolecular potential energy curves, along with the corresponding curve for the minimum energy C_s structure, should prove useful for undertaking MD and Monte Carlo simulations in condensed phases involving fluoride anions and ammonia.

V. Predicted infrared spectrum. The effects of complex formation on the ammonia molecule manifest themselves strongly in the vibrational modes. A stick spectrum produced from the calculated harmonic frequencies is presented in Fig. 4. Starting from low wavenumber, three bands are introduced corresponding to the intermolecular stretching and two intermolecular bending modes. To higher wavenumber are the bending modes of the ammonia molecule, in the 1000–2000 cm^{-1} range. The two bending modes of the bare ammonia with a_1 and e symmetry transform into three modes, two with a′ and one with a″ symmetry. The N–H stretching modes, in the 2500–3600 cm^{-1} range, are affected most by formation of the complex. Similar to the bending modes, the a_1 and *e* symmetry modes of bare ammonia transform into three modes, two with

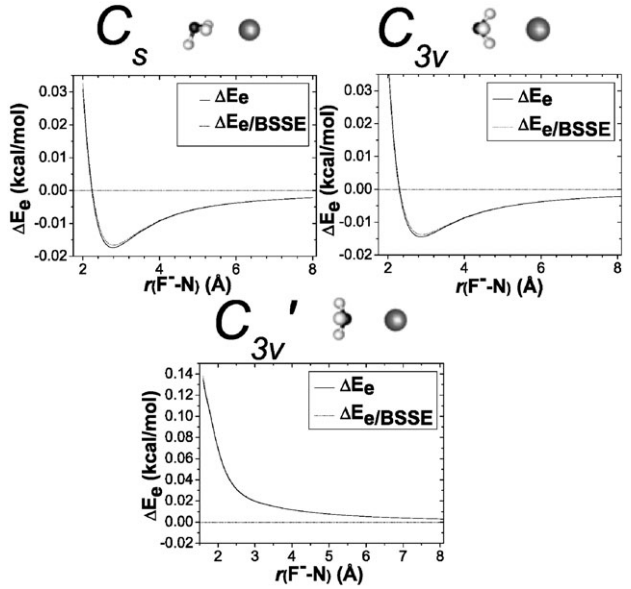

Fig. 3 Relaxed potential energy scans for the association of the fluoride and ammonia along the $r(F^-–N)$ coordinate. These curves correspond to the higher stationary points C_s and C_{3v}, and for the repulsive interaction with the fluoride approaching the nitrogen, labelled C_{3v}'. Data are provided in the supplementary material.†

a′ symmetry and one with a″ symmetry. One of these modes appears as the strong band located at 2685 cm^{-1}, and is due predominantly to motion of the H-bonded hydrogen. This band is shifted by 890 cm^{-1} to lower wavenumber from the centroid of the two calculated bare ammonia N–H stretches (Table 2), and has a marked increase in IR intensity (1615 km mol^{-1} in the complex *vs.* 8 and 3 km mol^{-1} for bare ammonia). Both of these effects are characteristic of hydrogen bond formation.[58] Two further vibrational modes, with very low IR intensity, are predicted to higher wavenumber and are due to the symmetric and antisymmetric vibrations of the non-bonded hydrogens. It is hoped that this data will be helpful for future experimental studies, however due to the large predicted binding energy of the complex (−15.8 kcal mol^{-1} or *ca.* 5315 cm^{-1}) vibrational predissociation spectroscopy is not applicable without resorting to the use of 'spy' atoms (recent examples can be found in refs. 38 and 59)

B. $F^-–(NH_3)_2$

The addition of a second ammonia to a fluoride anion results in ammonia–ammonia solvent interactions, which may lead to symmetric *versus* asymmetric solvation structures. With this in mind, we move now to the discussion of the 1 : 2 cluster, $F^-–(NH_3)_2$. Stationary points found from calculations at the MP2

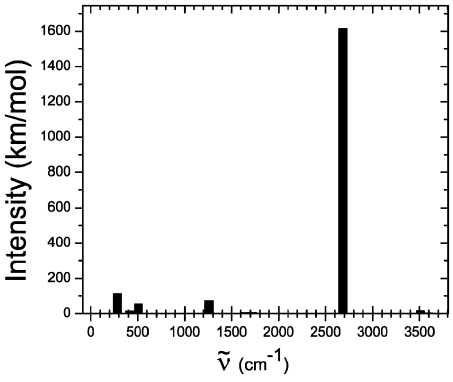

Fig. 4 Calculated IR spectrum of the $F^-–NH_3$ complex at the MP2/aug-cc-pVTZ level. Frequencies are provided in Table 2.

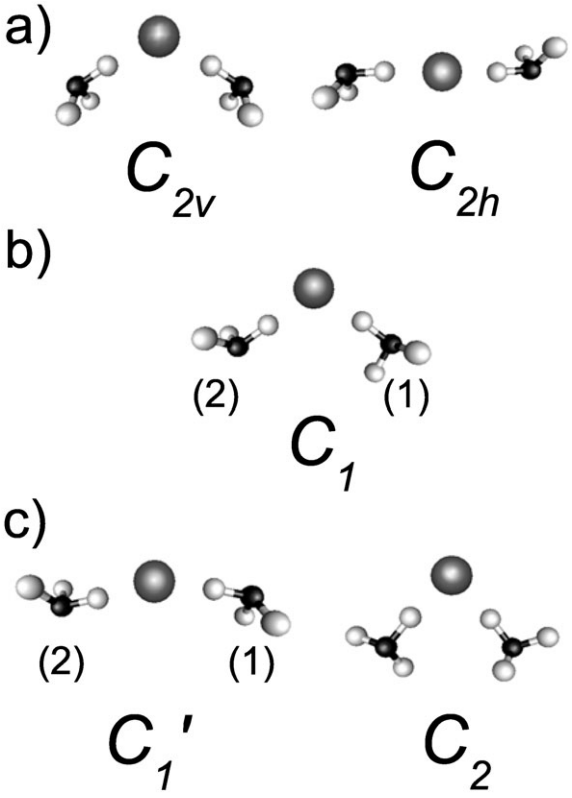

Fig. 5 Predicted structures for the $F^-–(NH_3)_2$ clusters. (a) C_{2v} and C_{2h} structures for both pVDZ and pVTZ; (b) C_1 structure for pVDZ, (c) C_2 and C_1' for pVTZ. Numbers in parentheses indicate non-equivalent ligands.

level with aug-cc-pVDZ and aug-cc-pVTZ basis sets are shown in Fig. 5. Two higher symmetry C_{2h} and C_{2v} structures (Fig. 5a) were predicted at both levels of theory. The C_1 symmetry structure, Fig. 5b, predicted from a MP2/aug-cc-pVDZ calculation converged to the C_2 structure shown in Fig. 5c when used as input for a MP2/aug-cc-pVTZ calculation. A fourth structure, with C_1 symmetry, was found from MP2/aug-cc-pVTZ calculations (henceforth labelled C_1'). When this stationary point was used as input in a MP2/aug-cc-pVDZ optimisation, it converged to the C_1 structure shown in Fig. 5b.

Optimised internal coordinates and calculated energies are provided in Table 3, highlighting the differences between the structures of the stationary points at the two levels of theory sampled. For common structures between the two levels of theory, the results indicate that increasing the basis set size has only a small effect on the internal coordinates. For the C_{2v} isomer, increasing the size of the basis set has no discernible effect on the structure (Table 3). For the C_{2h} structure, increasing the basis set size reduces the H-bonded N–H bond length, ($\Delta r \sim -0.01$ Å) and the intermolecular H-bonding angle ($\Delta\theta \sim -0.2°$). The most striking difference however between the two levels of theory is that this C_{2h} stationary point is predicted to be a minimum for aug-cc-pVDZ and a second order stationary point for aug-cc-pVTZ. From the discussion of the 1 : 1 complex, the pVTZ level is considered to be a better choice to describe these systems, however the differences in bond lengths and angles between the two levels of theory are not so large.

I. Structure descriptions and NBO analyses. The C_{2h} structure (Fig. 5a) has the two ammonias situated on opposite sides of a central fluoride anion, represents a symmetric type solvation structure. As stated previously, this structure is a minimum for the pVDZ calculations and a second order stationary point when the larger pVTZ basis set is used. The C_1' structure

Table 3 Calculated data for the stationary points of $F^-(NH_3)_2$ cluster at MP2/aug-cc-pVDZ and MP2/aug-cc-pVTZ levels of theory (aug-cc-pVTZ in bold). Provided are internal coordinates (r in Å and θ in degrees), *zpe* (in kcal mol^{-1}), MP2 energies (E_{MP2} in au), BSSE and *zpe* corrected energy differences ($\Delta E_{BSSE/Corr}$ in cal mol^{-1}), and for the minima the enthalpy changes for the ligand association reactions at 298 K ($\Delta H_{1\rightarrow 2}^{298}$ in kcal mol^{-1})

	C_{2h}		C_1'	$C_1 \rightarrow C_2$[a]		C_{2v}	
	aug-cc-pvdz	aug-cc-pvtz	aug-cc-pvtz	aug-cc-pvdz	aug-cc-pvtz	aug-cc-pvdz	aug-cc-pvtz
$r(F^-–H_b)$	1.677	**1.667**	**1.669 (1)**[b]	1.692 (1)[b]	**1.687**	1.667	**1.667**
			1.665 (2)	1.669 (2)			
$r(N–H_b)$	1.056	**1.050**	**1.050 (1)**	1.055 (1)	**1.048**	1.051	**1.051**
			1.051 (2)	1.058 (2)			
$r(N–H_t)$	1.023	**1.023**	**1.015 (1),(2)**	1.023 (1),(2)	**1.015**	1.015	**1.015**
$\theta(F^-–H_b–N)$	176.0	**175.8**	**176.0 (1)**	175.2 (1)	**173.2**	175.7	**175.7**
			175.7 (2)	177.1 (2)			
$\theta(H_b–N–H_t)$	104.9	**105.2**	**105.2 (1)**	104.8 (1),(2)	**105.7**	105.3	**105.3**
			105.3 (2)				
$\theta(H_t–N–H_t)$	104.4	**104.8**	**104.8 (1),(2)**	104.5 (1),(2)	**104.9**	104.8	**104.8**
$\theta(H_b–F^-–H_b)$	180.0	**180.0**	**156.4**	107.3	**83.7**	122.0	**122.0**
zpe	45.0	**45.2**	**45.2**	45.1	**45.6**	45.0	**45.2**
E_{MP2}	−212.523062	**−212.714818**	**−212.714834**	−212.523105	**−212.714588**	−212.523128	**−212.714754**
$\Delta E_{BSSE/Corr}$	(0)	**(0)**	**42**	137	**600**	68	**90**
$\Delta H_{1\rightarrow 2}^{298}$	−11.4	—	**−11.8**	−11.3	**−11.4**	—	—

[a] The C_1 structure (Fig. 5b) for aug-cc-pVDZ evolves to a C_2 structure (Fig. 5c) for aug-cc-pVTZ. [b] Numbers in parentheses indicate the non-equivalent ligands shown in Fig. 5.

(Fig. 5c) predicted from calculations with the pVTZ basis set is similar to the C_{2h} isomer, however the angle between the two ammonia molecules $\theta(H_b–F^-–Hb)$ is 156.4° compared to 180°. The ammonias are no longer equivalent, and have different H-bond lengths and angles, with $r(F^-–H_b) = 1.669$ and 1.665 Å and $\theta(F^-–H_b–N) = 176.0$ and 175.7°. This stationary point is a minimum at the MP2/aug-cc-pVTZ level of theory, and resembles a symmetric solvation structure.

The C_1 and C_2 structures (Fig. 5b and c) are minima, and feature both ammonias to one side of the fluoride anion, corresponding to an asymmetric type solvation structure. The difference between the two structures is that for C_2 the ammonias are equivalent, whereas for the C_1 structure the two ammonias have different H-bond lengths and angles (refer to Table 3). To determine whether H-bonding occurs between the two ammonias, NBO analyses were performed. The signature of an ammonia–ammonia H-bonding interaction is electron transfer from the nitrogen lone pairs of the proton acceptor to the σ^*(N–H) antibonding orbital of the proton donor. The NBO analyses reveal that there is no significant electron transfer, and hence the interactions cannot be considered true H-bonds. This is reflected in the geometries of the clusters. If there was a hydrogen bonding interact and transfer to the antibonding orbital, one should see an increased N–H bond length relative to the terminal N–H group. This is not observed (Table 3).

The third stationary point, with C_{2v} symmetry (Fig. 5a), is a first order transition state from calculations with both basis sets. The imaginary frequency for this structure corresponds to a concerted twisting of the ammonia molecules about the F^-–H_b–N axes. This isomer features both ammonias to one side of the anion, and hence can be thought of as an asymmetric type solvation structure.

As with the 1 : 1 complex, the geometry of the ammonia is perturbed from that of the bare molecule for both minima (refer to aug-cc-pVTZ calculations in Tables 2 and 3). Relative to bare ammonia, the N–H bond lengths associated with the hydrogen bound to the anion are elongated by *ca.* 0.04 Å, while the N–H bond lengths associated with free hydrogens are also longer by *ca.* 0.01 Å. The intramolecular H–N–H angles are smaller than in bare ammonia by roughly 1–2°. Compared with the 1 : 1 complex (Table 2, aug-cc-pVTZ results), the angle of the hydrogen bonds for the minima C_1' and C_2 are slightly further from linearity, with $\theta(F^-–H_b–N) = 176.0/175.7°$ and 173.2°, respectively, compared with 176.3° for the 1 : 1 complex. The intermolecular F^-–H_b bond lengths are increased, for example $\Delta r = +0.101$ Å for the C_2 isomer.

II. Cluster energies. One can see from the calculated energies at MP2/aug-cc-pVTZ presented in Table 3 that the energy differences between the stationary points are very small, and hence it is not possible to state conclusively which structure will be the preferred one. This situation is further clouded as the calculations predict that after BSSE and *zpe* corrections are made, the second order stationary point (C_{2h} symmetry) lies slightly lower in energy compared with the C_1' minimum. Obviously, at this level of theory the energies are not accurate enough, furthermore the value of the *zpe* from the *ab initio* calculations is derived using harmonic frequencies, and hence will also be a source of error. One can say, however, that at both levels of theory the symmetric type solvation structures are lower than the asymmetric ones, hinting that symmetric structures may be preferred. The dominant structure should be found by comparison of the predicted vibrational frequencies with experimental spectra (*vide infra*). We also calculated the enthalpy change for the ligand association reaction for both the C_1' and C_2 minima (MP2/aug-cc-pVTZ) as −11.8 and −11.4 kcal mol^{-1}, respectively. These are conservative values due to the aforementioned errors associated with the calculated *zpe*.

III. Predicted infrared spectra. Harmonic vibrational frequencies are given in Table 4, and stick spectra derived from the calculated vibrational frequencies are presented in Fig. 6. At low wavenumber (5–500 cm^{-1}) the bands are due to motion of ammonia ligands with respect to the anion and each other. These vibrations correspond to the intermolecular stretching, bending, rocking and wagging modes. To higher wavenumber, 1200–1700 cm^{-1}, lie the intramolecular bending vibrations of ammonia. The most obvious difference between the two isomers is seen in the highest frequency vibrations, corresponding to the N–H stretching modes (2900–3600 cm^{-1}).

The C_1' cluster features a very strong absorption around 2914 cm^{-1} (IR intensity = 2454 km mol^{-1}) due predominantly to the concerted antisymmetric motion of the two H-bonded hydrogens. The symmetric mode involving motion of these hydrogens is predicted to be considerably weaker (76 km mol^{-1}). In contrast for the C_2 isomer, two bands with

Table 4 Calculated harmonic vibrational frequencies for the four stationary points of F^-–$(NH_3)_2$ at the MP2/aug-cc-pVTZ level of theory. Also provided are mode symmetries and IR intensities in bold text (km mol^{-1})

Mode description[a]	C_2	C_1'	C_{2h}	C_{2v}
Inter.	25 *b* **60**	7 *a* **1**	13*i* b_u	33*i* a_2
Twisting and rocking	32 *a* **2**	11 *a* **8**	11*i* a_u	10 a_1
Modes	146 *a* **23**	20 *a* **88**	20 a_u	32 b_1
Symm. inter. stretch	221 *b* 57.7	203 *a* **4**	196 a_g	238 a_1
Anti. inter. stretch	273 *a* **68**	294 *a* **179**	299 b_u	267 b_2
Anti. inter. bend	379 *b* **39**	374 *a* **2**	373 b_g	375 a_2
Symm. inter. bend	403 *a* **7**	377 *a* **29**	375 a_u	382 b_1
Anti. inter. bend	473 *a* **78**	479 *a* **44**	477 b_u	475 b_2
Symm. inter. bend	474 *b* **52**	481 *a* **77**	479 a_g	488 a_1
Ammonia intra. bends	1216 *a* **27**	1227 *a* **76**	1224 b_u	1216 b_2
	1230 *b* **108**	1227 *a* **82**	1227 a_g	1235 a_1
	1651 *b* **13**	1652 *a* **14**	1652 b_u	1650 b_2
	1654 *a* **10**	1653 *a* **2**	1653 a_g	1654 a_1
	1709 *b* **38**	1722 *a* **11**	1721 a_u	1722 a_2
	1753 *a* **0**[b]	1725 *a* **0**[b]	1725 b_g	1725 b_1
Anti. H-bonded N–H stretch	2944 *b* **921**	2914 *a* **2454**	2916 b_u	2903 b_2
Symm. H-bonded N–H stretch	3033 *a* **957**	3003 *a* **76**	3005 a_g	2992 a_1
Non-bonded N–H	3521 *b* **13**	3523 *a* **32**	3523 b_u	3522 b_2
Stretches	3521 *a* **16**	3523 *a* **2**	3523 a_g	3523 a_1
	3607 *b* **1**	3609 *a* **1**	3609 b_g	3609 a_2
	3607 *a* **0**[b]	3609 *a* **1**	3609 a_u	3609 b_1

[a] inter. = intermolecular, intra. = intramolecular, symm. = symmetric, anti = antisymmetric. [b] These IR intensities were less than 1 km mol^{-1}, however were not inactive.

appreciable intensity are predicted at 2944 and 3033 cm^{-1} (IR intensity = 921 and 957 kJ mol^{-1}, respectively) due to the antisymmetric and symmetric motion of the bound hydrogens, respectively. It is hoped that these spectra will prove valuable for the interpretation of future experimental studies. Unfortunately, as with the 1 : 1 F^-–NH_3 complex, predissociation spectroscopy can not be applied to the 1 : 2 cluster as the predicted binding energy of the second ligand of *ca.* 4130 cm^{-1} exceeds the energy imparted to the molecule by an IR photon following vibrational excitation of the N–H stretching modes.

C. F^-–$(NH_3)_3$

The F^-–$(NH_3)_3$ clusters were studied at the MP2/aug-cc-pVDZ level of theory, as this level was shown to produce structures that were quite similar to the higher MP2/aug-cc-pVTZ level when used for F^-–$(NH_3)_2$. To illustrate this point, the C_3 symmetry isomer found for F^-–$(NH_3)_3$ was trialled at the MP2/aug-cc-pVTZ level. The differences in bond lengths and angles are <0.008 Å and $<0.9°$, respectively (see Table 5)

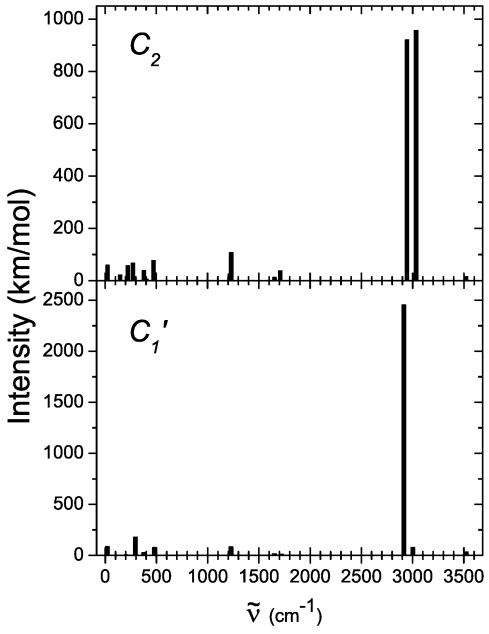

Fig. 6 Calculated IR spectra for the two minima of F^-–$(NH_3)_2$ at the MP2/aug-cc-pVTZ level. Frequencies and band symmetries are provided in Table 4.

I. Structure descriptions. Four stationary points, shown in Fig. 7, were found for the F^-–$(NH_3)_3$ cluster at the MP2/aug-cc-pVDZ level of theory. Calculated data and harmonic vibrational frequencies are provided in Tables 5 and 6. The four stationary points correspond to a highly symmetric C_{3h} structure with three equivalent ammonia ligands (symmetric solvation), a C_3 isomer featuring a pyramid of ammonia ligands that are bound to each other (asymmetric solvation), a C_1 asymmetric structure with three non-equivalent ligands on one side of the anion (asymmetric solvation), and a C_s or 'ring' isomer which features two ammonias bound to the anion, and a third further out bound to these two (asymmetric solvation). At the MP2/aug-cc-pVDZ level the four stationary points are minima with all real vibrational frequencies. This is in contrast to the predictions for the analogous F^-–$(H_2O)_3$ clusters, where only three structures are observed and the symmetric C_{3h} structure is a higher order stationary point.[28,34] It is, of course, possible that at higher levels of theory some of the stationary points may no longer be minima as found for the F^-–$(NH_3)_2$ cluster. Differences in the predicted infrared spectra should allow experimentalists to determine which structure is preferred (*vide infra*).

Distortions of the ammonia ligands are evident from association with the fluoride anion, however they are generally less perturbed than in the F^-–$(NH_3)_2$ clusters. The N–H bond lengths are elongated relative to the calculated structure of bare ammonia, with r(N–H_b) = 1.05 Å compared with r(N–H) = 1.02 Å (aug-cc-pVDZ results, Table 2). The intramolecular ammonia angles θ(H–N–H) are smaller than in bare ammonia, with θ(H–N–H) in the cluster generally in the 103–106° range, compared with θ(H–N–H) = 106.3°. The linearity of the anion –ammonia hydrogen bonds differs between the isomers of F^-–$(NH_3)_3$ and F^-–$(NH_3)_2$.

II. Cluster energies. The energetic ordering of the isomers, after BSSE and zero point energy difference corrections are

Table 5 Calculated data of the stationary points of F^-–$(NH_3)_3$ at the MP2/aug-cc-pVDZ level of theory. Provided are internal coordinates (r in Å and θ in deg.), *zpe* (in kcal mol^{-1}), MP2 energies (E_{MP2} in au), energy differences corrected for BSSE and *zpe* ($\Delta E_{BSSE/Corr}$ in kcal mol^{-1}), and incremental association enthalpy changes with respect to the most stable F^-–$(NH_3)_2$ isomer at MP2/aug-cc-pVDZ ($\Delta H_{2\rightarrow3}^{298}$ in kcal mol^{-1})

	C_{3h}	C_3[a]	C_1[b]	C_s[c]
$r(F^-–H_b)$	1.732	1.780 (−5)	1.804 (**1**)	1.654 *B*
			1.714 (**2**)	3.439 *S*
			1.757 (**3**)	
$r(N–H_b)$	1.048	1.044 (−6)	1.042 (**1**)	1.057 *B*
			1.050 (**2**)	1.028 *S*
			1.046 (**3**)	
$r(N–H_{ba})$[d]		1.024 (−8)	1.023 (**1**)	1.028 *S*
$r(N–H_t)$	1.022	1.022 (−8)	1.022	1.022
$\theta(F^-–H_b–N)$	176.2	167.9 (−3)	168.1 (**1**)	179.7 *B*
			177.7 (**2**)	114.2 *S*
			171.8 (**3**)	
$\theta(H_b–N–H_t)$	104.9	105.8 (+3)	104.2 (**1**)	105.8 *B*
			103.2 (**1**)	105.7 *B*
			105.3 (**2**)	105.0 *S*
			105.6 (**2**)	
			103.9 (**3**)	
			105.4 (**3**)	
$\theta(N–H_{ba}–N)$[d]		120.1 (0)	117.6 (**1**),(**2**)	166.1
$\theta(H_t–N–H_t)$	104.5		104.2 (**1**)	105.0
			104.9 (**2**)	
			104.8 (**3**)	
$\theta(H_b–F^-–H_b)$	120.0	80.5 (+9)	81.8 (**1–2**)	109.8
			86.7 (**2–3**)	
			88.0 (**3–1**)	
zpe	68.0	69.1	68.5	68.8
E_{MP2}	−268.947163	−268.948353	−268.947620	−268.944931
$\Delta E_{BSSE/Corr}$	(0.0)	1.3	1.0	3.1
$\Delta H_{2\rightarrow3}^{298}$	−9.6	−9.0	−9.1	−7.1

[a] Numbers in parentheses are differences in last sig. fig. for the equivalent structure optimised at MP2/aug-cc-pVTZ. [b] (**1**), (**2**) and (**3**) correspond to the three non-equivalent ammonia molecules (Fig. 7). [c] *B* are the ammonias bound to the anion, *S* is the satellite ammonia removed from the anion (Fig. 7). [d] H_{ba} refers to the hydrogen involved in an ammonia–ammonia bond.

taken into account, is $C_{3h} < C_1 < C_3 < C_s$. Unlike the F^-–$(NH_3)_2$ clusters, the difference in the energies of the isomers is appreciable (greater than 1 kcal mol^{-1}), which may hint at a basis set size effect. Similar to the F^-–$(NH_3)_2$ clusters the accuracy of these energies is questionable as firstly the zero point energy used in the calculation is derived from the calculated harmonic frequencies, and secondly the use of the aug-cc-pVDZ basis set may not be adequate. This said however, it appears that symmetric solvation structure with C_{3h} symmetry is favoured. The calculated enthalpy changes for association of a third ammonia ligand are −9.3, −9.0, −9.1, and −7.1 kcal mol^{-1} for the C_{3h}, C_3, C_1, and C_s isomers, respectively. These values are calculated with respect to the most stable isomer from MP2/aug-cc-pVDZ calculations of F^-–$(NH_3)_2$, which was the C_{2h} structure.

III. NBO analyses. NBO analyses were performed for each stationary point to determine the extent, if any, of hydrogen bonding between the ammonia solvent molecules. Obviously, there should be no significant H-bonding interaction in the C_{3h} isomer as the ammonias are pointing away from one another. This is revealed in the NBO analysis, with no evidence for $lp_N \rightarrow \sigma^*_{N–H}$ electron density transfer. There is, however, some evidence of H-bonding between the ammonia ligands for the remaining three isomers. Firstly, for the C_3 isomer, the NBO analysis reveals *ca.* 1.0 *me* of electron density transfer from a lone pair of each nitrogen into the $\sigma^*_{N–H}$ orbital of the neighbouring ammonia. The second-order perturbation energy, or stabilisation energy, for the density transfer is predicted to be $E^{(2)} = 0.35$ kcal mol^{-1}. For the C_1 isomer, *ca.* 0.5 *me* is transferred from a lone pair of the nitrogen of ammonia (2) to the $\sigma^*_{N–H}$ of ammonia (1), with the second-order perturbation energy being $E^{(2)} = 0.12$ kcal mol^{-1}. There is no evidence for an H-bonding interaction between ammonia (2) and ammonia (3). Finally, for the C_s 'ring' isomer, the NBO analysis predicts that 9.4 *me* is transferred from a lone pair of the nitrogens of both *B* ammonias to the $\sigma^*_{N–Hba}$ orbitals of the *S* ammonia. In this case, the stabilisation energy is quite

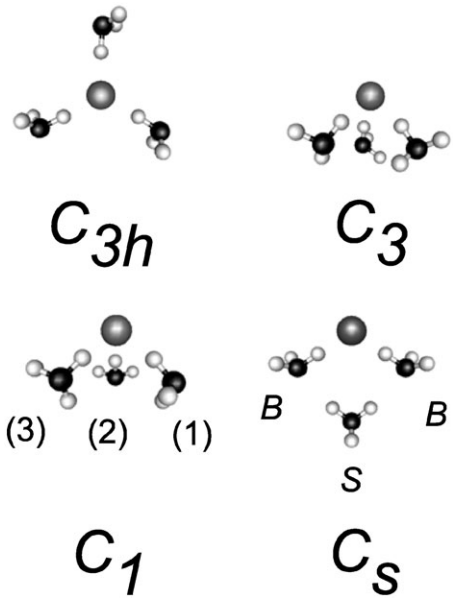

Fig. 7 Four predicted stationary points for the F^-–$(NH_3)_3$ cluster at the MP2/aug-cc-pVDZ level of theory. All four isomers are minima, with the symmetric C_{3h} structure being the global minimum at this level of theory. Optimal internal coordinates appear in Table 5.

Table 6 Calculated harmonic vibrational frequencies for the four isomers of F^-–$(NH_3)_3$ at the MP2/aug-cc-pVDZ level of theory. Also provided are IR intensities in bold text (km mol^{-1}) and mode symmetries

Mode description[a]	C_{3h}	C_3	C_1	C_s[b]
Inter.	14 *a″* **130**	67 *e* **5**	21 *a* **3**	28 *a′* **16**
Wagging,	16 *e′* **3**	71 *a* **6**	30 *a* **4**	52 *a′* **10**
Twisting,	23 *e″* **0**	150 *e* **40**	47 *a* **1**	63 *a″* **6**
Rocking	32 *a″* **4**	242 *a* **18**	73 *a* **21**	91 *a′* **36**
Modes			125 *a* **30**	121 *a″* **4**
			166 *a* **65**	
Anti. inter. stretches	253 *e′* **81**	199 *e* **35**	200 *a* **36**	270 *a″* **58**
			216 *a* **33**	
Symm. inter. stretches	186 *a′* **0**	266 *a* **55**	265 *a* **42**	151 *a′* **2** *S*
				258 *a′* **39** *B*
Inter. bends	343 *e″* **0**	352 *e* **24**	333 *a* **21**	293 *a′* **71**
	351 *a″* **44**	383 *a* **5**	347 *a* **20**	300 *a″* **55**
	451 *a′* **0**	461 *e* **71**	368 *a* **23**	370 *a″* **0**[c]
	461 *e′* **104**	468 *a* **117**	423 *a* **72**	386 *a′* **33**
			448 *a* **69**	424 *a″* **1**
			485 *a* **90**	522 *a′* **30**
				532 *a″* **139**
Ammonia intra. bends	1200 *a′* **0**	1197 *a* **58**	1197 *a* **138**	1190 *a′* **116**
	1219 *e′* **112**	1230 *e* **84**	1231 *a* **102**	1226 *a″* **16**
	1635 *a′* **0**	1632 *a* **13**	1221 *a* **23**	1245 *a′* **113**
	1638 *e′* **11**	1637 *e* **1**	1631 *a* **11**	1629 *a″* **6**
	1699 *e″* **0**	1694 *e* **52**	1638 *a* **7**	1630 *a′* **1**
	1704 *a″* **14**	1732 *a* **0**[c]	1646 *a* **14**	1658 *a″* **5**
			1688 *a* **15**	1695 *a′* **4**
			1702 *a* **17**	1699 *a″* **0**[c]
			1721 *a* **4**	1705 *a′* **12**
Anti.	3079 *e′* **1309**	3138 *e* **484**	3046 *a* **756**	2895 *a″* **1697***B*
H-bonded N–H stretches			3136 *a* **590**	3389 *a′* **123***S*
Symm.	3159 *a″* **0**	3215 *a* **598**	3222 *a* **497**	2982 *a′* **452***B*
H-bonded N–H stretches				3496 *a″* **188***S*
Non-bonded	3513 *e′* **36**	3505 *e* **1**	3508 *a* **17**	3511 *a″* **9***B*
N–H stretches	3514 *a′* **0**	3507 *a* **58**	3509 *a* **14**	3512 *a′* **42***B*
	3599 *e″* **0**	3594 *e* **4**	3512 *a* **31**	3582 *a′* **20***S*
	3599 *a″* **3**	3595 *a* **1**	3590 *a* **0**[c]	3603 *a″* **0**[c]*B*
			3596 *a* **1**	3603 *a′* **2***B*
			3600 *a* **1**	

[a] inter. = intermolecular, intra. = intramolecular, symm. = symmetric, anti = antisymmetric. [b] *B* corresponds to the ammonias bound to the anion, *S* to the satellite ammonia removed from the anion (Fig. 7). [c] These IR intensities were less than 1 km mol^{-1}, however were not inactive.

large $E^{(2)} = 6.2$ kcal mol^{-1}, which is understandable as it is the ammonia–ammonia H-bonds between the *S* and *B* ammonias which form the 'ring' structure.

The strengths of the H-bonds are reflected in the isomer structures. The C_s isomer features the strongest ammonia–ammonia H-bond, and hence the N–H bond length of the proton donor is somewhat longer than the terminal N–H bonds (r(N–H) = 1.028 Å *versus* 1.022 Å). The second strongest ammonia–ammonia H-bond is seen in the C_3 isomer, and in this case the proton donor N–H bond lengths are 1.024 Å compared with 1.022 Å for the terminal N–H bonds. Finally, the C_1 isomer features the weakest H-bond, and the difference is 1.023 Å *vs.* 1.022 Å.

While the ammonia–ammonia interactions can be called H-bonds due to the predicted electron density transfer, they are certainly much weaker than the H-bond formed between the anion and the ammonia molecules. For example, from the NBO analysis for the C_3 isomer, the stabilisation energy provided from electron density transfer from the lone pairs of the fluoride anion to the ammonia ligand (Total $lp_F \rightarrow \sigma^*_{N-H}$) is approximately 20 kcal mol^{-1}, and the occupancy of the σ^*_{N-Hb} orbital is on the order of 28 *me*.

IV. Predicted infrared spectra. The results of vibrational frequency calculations for the four isomers are provided in Table 6, and shown as stick spectra in Fig. 8. As with the F^-–$(NH_3)_2$ cluster, the vibrations can be placed into three groups. At low wavenumber are the intermolecular vibrations (15–530 cm^{-1}), at intermediate wavenumber are the bending vibrations of the ammonia ligands (1190–1720 cm^{-1}), and at higher wavenumber the N–H stretching modes (2895–3600 cm^{-1}). Looking to this N–H stretch region, there are distinct differences in the band positions and intensities which should prove useful for analysis of experimental spectra. Firstly, for the most stable C_{3h} symmetry isomer, only one N–H stretching mode has appreciable IR intensity. This mode corresponds predominantly to the concerted antisymmetric motion of the H-bonded hydrogens. For the C_3 isomer, two bands are predicted at 3138 and 3215 cm^{-1}, corresponding to the antisymmetric and symmetric motion of the H-bonded hydrogens, respectively. For the C_1 isomer, three bands are predicted at 3046, 3136, and 3222 cm^{-1}. The first two bands correspond to concerted antisymmetric motion of the bound hydrogens, while the third is due to their symmetric motion. The C_s isomer is an interesting case, as two strong bands are predicted at 2895 and 2982 cm^{-1} corresponding to the antisymmetric and symmetric motion of the hydrogens bound to the anion (*B*). Two weaker bands are predicted at 3389 and 3496 cm^{-1}, corresponding to symmetric and antisymmetric motion of the hydrogens of the satellite ammonia forming the ammonia–ammonia hydrogen bonds to the two ammonias bound to the fluoride anion (see Fig. 7).

The calculations predict that the binding energies of the third ammonia ligands to the C_{3h}, C_3, and C_1 isomers are around

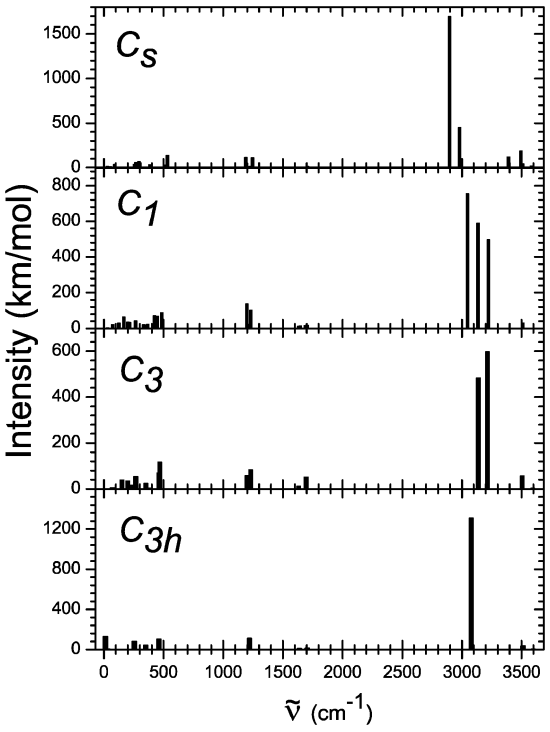

Fig. 8 Calculated IR spectrum of the four isomers of $F^-(NH_3)_3$ at the MP2/aug-cc-pVDZ level. Frequencies also provided in Table 6.

3200–3400 cm^{-1} (Table 5). While these binding energies are still higher than the predicted H-bonded N–H stretching frequencies, it may be possible to apply vibrational predissociation spectroscopy to complexes which have several low wavenumber intermolecular vibrational levels populated, *i.e.* vibrationally warm complexes. Spectra obtained *via* argon predissociation spectroscopy would be preferable as the complexes would be locked into the minimum energy conformation. The binding energy of the third ammonia to the C_s isomer is predicted to be lower, at *ca.* 2480 cm^{-1}. The predicted H-bonded N–H stretching modes are higher than this value, and hence this cluster should be amenable to vibrational predissociation spectroscopy, without resorting to argon predissociation.

4. Summary

The structures, binding energies, and vibrational spectra of small fluoride–ammonia clusters have been investigated *via ab initio* calculations. The F^-–NH_3 complex features a single hydrogen bond, and has C_s symmetry. The predicted binding energy for this complex is 15.8 kcal mol^{-1} or 5525 cm^{-1}. Two minimum energy structures with C_2 and C_1 symmetry were found for the F^-–$(NH_3)_2$ cluster from MP2/aug-cc-pVTZ calculations. While the predicted energy separations of the isomers are quite small, differences in the predicted infrared spectra should help experimentalists determine the preferred structure. Finally, four isomers were predicted for the F^-–$(NH_3)_3$ cluster from MP2/aug-cc-pVDZ calculations. The symmetric C_{3h} isomer was found to be lowest in energy, indicating that symmetric solvation was more likely than asymmetric solvation. The predicted binding energy of the third ammonia ligand was estimated to be *ca.* 9.6 kcal mol^{-1} or 3360 cm^{-1} for the most stable isomer. Again, comparison with experimental spectra should help define the most probable structure.

Acknowledgements

We thank Zoë Loh (Melbourne University) for useful preliminary discussions, Martin Fechner (MPI) for computer assistance, the MPI für Biophysikalische Chemie and the Alexander von Humboldt Foundation for financial support.

References

1 J. V. Coe, *Int. Rev. Phys. Chem.*, 2001, **20**, 33.
2 S. Nandi, A. Sanov, N. Delaney, J. Faeder, R. Parson and W. C. Lineberger, *J. Phys. Chem. A*, 1998, **102**, 8827.
3 M. E. Nadal, P. D. Kleiber and W. C. Lineberger, *J. Chem. Phys.*, 1996, **105**, 504.
4 C. A. Corbett, T. J. Martinez and J. M. Lisy, *J. Phys. Chem. A*, 2002, **106**, 10015.
5 M. Ichihashi, Y. Sadanaga, J. M. Lisy and T. Kondow, *Chem. Lett.*, 2000, **11**, 1240.
6 O. M. Cabarcos, C. J. Weinheimer, T. J. Martinez and J. M. Lisy, *J. Chem. Phys.*, 1999, **110**, 9516.
7 W. H. Robertson, K. Karapetian, P. Ayotte, K. D. Jordan and M. A. Johnson, *J. Chem. Phys.*, 2002, **116**, 4853.
8 W. H. Robertson, E. G. Diken, E. A. Price, J. W. Shin and M. A. Johnson, *Science (Washington, D. C.)*, 2003, **299**, 1367.
9 S. B. Nielsen, P. Ayotte, J. A. Kelley and M. A. Johnson, *J. Chem. Phys.*, 1999, **111**, 9593.
10 E. J. Bieske, *Chem. Soc. Rev.*, 2003, **32**, 231.
11 D. A. Wild, P. J. Milley, Z. M. Loh, P. S. Weiser and E. J. Bieske, *Chem. Phys. Lett.*, 2000, **323**, 49.
12 D. A. Wild, P. S. Weiser, E. J. Bieske and A. Zehnacker, *J. Chem. Phys.*, 2001, **115**, 824.
13 D. A. Wild, Z. M. Loh, R. L. Wilson and E. J. Bieske, *J. Chem. Phys.*, 2002, **117**, 3256.
14 S. A. Nizkorodov, O. Dopfer, T. Ruchti, M. Meuwly, J. P. Maier and E. J. Bieske, *J. Phys. Chem.*, 1995, **99**, 17118.
15 M. S. Johnson, K. T. Kuwata, C. K. Wong and M. Okumura, *Chem. Phys. Lett.*, 1996, **260**, 551.
16 J. H. Choi, K. T. Kuwata, Y. B. Cao and M. Okumura, *J. Phys. Chem. A*, 1998, **102**, 503.
17 J. H. Choi, K. T. Kuwata, B. M. Haas, Y. B. Cao, M. S. Johnson and M. Okumura, *J. Chem. Phys.*, 1994, **100**, 7153.
18 K. Seki, Y. Sumiyoshi and Y. Endo, *Chem. Phys. Lett.*, 2000, **331**, 184.
19 Y. Ohshima, Y. Sumiyoshi and Y. Endo, *J. Chem. Phys.*, 1997, **106**, 2977.
20 S. T. Arnold, J. H. Hendricks and K. H. Bowen, *J. Chem. Phys.*, 1995, **102**, 39.
21 J. H. Hendricks, H. L. de Clercq, C. B. Freidhoff, S. T. Arnold, J. G. Eaton, C. Fancher, S. A. Lyapustina, J. T. Snodgrass and K. H. Bowen, *J. Chem. Phys.*, 2002, **116**, 7926.
22 N. L. Pivonka, T. Lenzer, M. R. Furlanetto and D. M. Neumark, *Chem. Phys. Lett.*, 2001, **334**, 24.
23 T. Lenzer, I. Yourshaw, M. R. Furlanetto, N. L. Pivonka and D. M. Neumark, *J. Chem. Phys.*, 2001, **115**, 3578.
24 S. Roszak and J. Leszczynski, *J. Phys. Chem.A*, 2003, **107**, 949.
25 P. Botschwina, T. Dutoi, M. Mladenovic, R. Oswald, S. Schmatz and H. Stoll, *Faraday Discuss.*, 2001, **118**, 433.
26 A. V. Nemukhin, A. A. Granovsky and D. A. Firsov, *Mendeleev Commun.*, 1999, **6**, 215.
27 H. H. Ritze, *Chem. Phys. Lett.*, 1997, **275**, 399.
28 O. M. Cabarcos, C. J. Weinheimer, J. M. Lisy and S. S. Xantheas, *J. Chem. Phys.*, 1999, **110**, 5.
29 P. Ayotte, G. H. Weddle and M. A. Johnson, *J. Chem. Phys.*, 1999, **110**, 7129.
30 P. Ayotte, C. G. Bailey, G. H. Weddle and M. A. Johnson, *J. Phys. Chem. A*, 1998, **102**, 3067.
31 G. M. Chaban, S. S. Xantheas and R. B. Gerber, *J. Phys. Chem. A*, 2003, **107**, 4952.
32 M. Masamura, *J. Phys. Chem. A*, 2002, **106**, 8925.
33 M. Masamura, *J. Chem. Phys.*, 2003, **118**, 6336.
34 S. S. Xantheas and T. H. Dunning Jr., *J. Phys. Chem.*, 1994, **98**, 13489.
35 S. S. Xantheas and L. X. Dang, *J. Phys. Chem.*, 1996, **100**, 3989.
36 F. N. Keutsch, J. D. Cruzan and R. J. Saykally, *Chem. Rev.*, 2003, **103**, 2533.
37 F. Huisken, M. Kaloudis and A. Kulcke, *J. Chem. Phys.*, 1996, **104**, 17.
38 W. H. Robertson and M. A. Johnson, *Ann. Rev. Phys. Chem.*, 2003, **54**, 173.
39 D. H. Evans, R. G. Keesee and A. W. Castleman Jr., *J. Chem. Phys.*, 1987, **86**, 2927.
40 U. Kaldor, *Z. Phys. D: A., Mol. Clusters*, 1994, **31**, 279.
41 G. Markovich, O. Cheshnovsky and U. Kaldor, *J. Chem. Phys.*, 1993, **99**, 6201.

42 P. S. Weiser, D. A. Wild, P. P. Wolynec and E. J. Bieske, *J. Phys. Chem. A*, 2000, **104**, 2562.
43 C. Frischkorn, M. T. Zanni, A. V. Davis and D. M. Neumark, *Faraday Discuss.*, 2000, **115**, 49.
44 R. Ayala, J. M. Martinez, R. R. Pappalardo and E. S. Marcos, *J. Chem. Phys.*, 2003, **119**, 9538.
45 S. S. Xantheas, *J. Phys. Chem.*, 1996, **100**, 9703.
46 P. Weis, P. R. Kemper, M. T. Bowers and S. S. Xantheas, *J. Am. Chem. Soc.*, 1999, **121**, 3531.
47 J. S. Lee and S. Y. Park, *Chem. Phys. Lett.*, 2000, **112**, 230.
48 R. A. Kendall, T. H. Dunning and R. J. Harrison, *J. Chem. Phys.*, 1992, **96**, 6796.
49 D. E. Woon and T. H. Dunning, *J. Chem. Phys.*, 1993, **98**, 1358.
50 T. H. Dunning, *J. Chem. Phys.*, 1989, **90**, 1007.
51 S. F. Boys and F. Bernardi, *Mol. Phys.*, 1970, **19**, 553.
52 A. E. Reed, L. A. Curtiss and F. Weinhold, *Chem. Rev.*, 1988, **88**, 899.
53 J. E. Del Bene, H. D. Mettee, M. J. Frisch, B. T. Luke and J. A. Pople, *J. Phys. Chem.*, 1983, **87**, 3279.
54 M. J. Frisch, G. W. Trucks, H. B. Schlegel, G. E. Scuseria, M. A. Robb, J. R. Cheeseman, J. A. Montgomery, T. V. Jr., K. N. Kudin, J. C. Burant, J. M. Millam, S. S. Iyengar, J. Tomasi, V. Barone, B. Mennucci, M. Cossi, G. Scalmani, N. Rega, G. A. Petersson, H. Nakatsuji, M. Hada, M. Ehara, K. Toyota, R. Fukuda, J. Hasegawa, M. Ishida, T. Nakajima, Y. Honda, O. Kitao, H. Nakai, M. Klene, J. E. K. X. Li, H. P. Hratchian, J. B. Cross, C. Adamo, J. Jaramillo, R. Gomperts, R. E. Stratmann, O. Yazyev, A. J. Austin, R. Cammi, C. Pomelli, J. W. Ochterski, P. Y. Ayala, K. Morokuma, G. A. Voth, P. Salvador, J. J. Dannenberg, V. G. Zakrzewski, S. Dapprich, A. D. Daniels, M. C. Strain, O. Farkas, D. K. Malick, A. D. Rabuck, K. Raghavachari, J. B. Foresman, Q. C. J. V. Ortiz, A. G. Baboul, S. Clifford, J. Cioslowski, B. B. Stefanov, G. Liu, A. Liashenko, P. Piskorz, I. Komaromi, R. L. Martin, D. J. Fox, T. Keith, M. A. Al-Laham, C. Y. Peng, A. Nanayakkara, M. Challacombe, P. M. W. Gill, B. Johnson, W. Chen, M. W. Wong, C. Gonzalez and J. A. Pople, *GAUSSIAN 03 (Revision B.04)*, Gaussian, Inc., Pittsburgh PA, 2003.
55 L. Laaksonen, *J. Mol. Graph.*, 1992, **10**, 33.
56 D. L. Bergman and L. Laaksonen, *J. Mol. Graph.*, 1997, **15**, 301.
57 G. Herzberg, *Molecular Spectra and Molecular Structure II: Infrared and Raman Spectra of Polyatomic Molecules*, Krieger, Malabar, Vol. 2, 1991.
58 G. C. Pimentel and A. L. McClellan, *The Hydrogen Bond*, W. H. Freeman, New York, 1960.
59 D. A. Wild, Z. M. Loh, R. L. Wilson and E. J. Bieske, *Chem. Phys. Lett.*, 2003, **369**, 684.

